Mechanisms for Thermal Conduction in Hydrogen Hydrate

Niall J. English[1,2,a)], Paul D. Gorman[1] and J.M.D. MacElroy[1,2]

[1]*The SFI Strategic Research Cluster in Solar Energy Conversion, School of Chemical and Bioprocess Engineering and* [2]*Centre for Synthesis and Chemical Biology University College Dublin, Belfield, Dublin 4, Ireland.*

Keywords: Molecular Dynamics, Thermal Conductivity, Green-Kubo, Hydrogen Hydrate

Extensive equilibrium molecular dynamics (MD) simulations have been performed to investigate thermal conduction mechanisms via the Green-Kubo approach for (type II) hydrogen hydrate, at 0.05 kbar and between 30 and 250 K, for both lightly-filled H_2 hydrates (1s4l) and for more densely-filled H_2 systems (2s4l), in which four H_2 molecules are present in the large cavities, with respective single- and double-occupation of the small cages. The TIP4P water model was used in conjunction with a fully atomistic hydrogen potential along with long-range Ewald electrostatics. It was found that substantially less damping in guest-host energy transfer is present in hydrogen hydrate as is observed in common type I clathrates (*e.g.*, methane hydrate), but more akin in to previous results for type II and H methane hydrate polymorphs. This gives rise to larger thermal conductivities relative to common type I hydrates, and also larger than type II and H methane hydrate polymorphs, and a more crystal-like temperature dependence of the thermal conductivity.

[a)] Corresponding author. Tel: +35317161646. Email: niall.english@ucd.ie

INTRODUCTION

Gas hydrates are crystalline inclusion compounds with a H_2O lattice that forms a periodic array of cages with each cage large enough to contain a gas molecule [1,2]. There are three known hydrate structures: sI, sII and sH. Given our interest in hydrogen and tetrahydrofuran sII hydrates in this study, a unit cell in sII [3] hydrate consists of 136 water molecules forming 16 small cages and 8 large cages. The small cages are pentagonal dodecahedral (5^{12}) and the large cages are hexadecahedral ($5^{12}6^4$). Each 5^{12} cage may contain one, or possibly two, H_2 molecules, while each $5^{12}6^4$ cage may contain up to four H_2 molecules [4].

The possibility of using sII hydrates for hydrogen storage has been studied extensively [5-7]. The extreme pressure needed to form pure hydrogen hydrate has been a limiting factor and has led to the study of mixed stabiliser-H_2 hydrates [8-10], in the hope is that a stabilising compound will allow hydrate formation at lower pressures. Hydrates stabilised by THF, for instance, have attracted interest in this respect as they have been reported to be stable at close to room temperature, and at much lower pressures than pure hydrogen-hydrate [4,5,8,11]. Although the concept of large-scale seasonal storage is not new [12,13], the proposition of using mixed THF-H_2 hydrate for such efforts [14] is attractive, as it is a completely reversible physical hydrogen storage material. However, the exact weight percentage of hydrogen in such a system is still disputed, with estimates ranging from 1-4 wt% H_2 [8,14] greatly affecting its viability as a storage medium. It is understood that hydrate structures which enable multiple occupancy of hydrogen will likely be required for clathrate hydrates to be practical hydrogen storage medium. Ref. 15 presents part of a Tokyo-based feasibility study of on the large-scale *in situ* storage of hydrogen in the form of clathrate hydrates, in which it is concluded that a large portion of the energy that

could be extracted from the hydrogen-hydrate would be needed to power the refrigeration required. However, their industrial design does not address the possibility of the geologic storage of hydrates where lower temperatures may be achieved at a lower energy cost [15].

An important parameter governing the viability of large-scale hydrogen storage, whether in pure form or with a stabiliser added for greater lower-pressure stability, is the thermal conductivity, particularly if it is desired to use thermal heating to release hydrogen via dissociation of hydrogen hydrates. Naturally, the thermal conductivity also affects the kinetics of hydrogen hydrate formation substantially, which is also key in assessing the feasibility of large-scale storage. To the knowledge of the authors, there have been no reports of measurements or predictions of thermal conductivity of hydrogen hydrate, and therefore this study is addressed at predicting thermal conductivity and elucidating mechanisms contributing thereto in hydrogen hydrates as a necessary first step towards the more ambitious longer-term goal of predictive, *in silico* design of mixed-H_2 hydrates with desirable thermal conduction properties.

The most peculiar property of common (type I) hydrates, *e.g.*, methane hydrate, is its very low thermal conductivity compared to ice. Moreover, above around 100 K, its conductivity displays a weak temperature dependence, resembling amorphous solids [16,17]. This anomalous "glasslike" thermal conductivity behaviour is shared by some clathrate-like compounds, e.g. metal-Si clathrates [18] and skutterudites [19]. Several hypotheses have been suggested to explain this observation, the most studied being the "resonant scattering" model [16,20-23], which originates in hydrates from "avoided-crossings" of lattice acoustic phonons with localised guest vibrations of identical symmetry [21-23] dissipating heat transport. Experimental measurements of thermal conductivity in (type I) methane hydrate exhibit a crystal-like temperature

dependence below 90 K, with glass-like behaviour above this temperature [24], while similar low-temperature behaviour is observed in some semi-conductor clathrates [25]. In addition to various recent molecular dynamics (MD) studies estimating methane hydrate thermal conductivities [26-34], and those of other clathrates [29,34], progress has been made towards elucidating the underlying mechanisms governing thermal conduction in methane hydrates of various polymorphs [31-33]. It was found that a greater extent of damping in guest-host energy transfer in type I methane hydrates as higher temperatures (above 150 K), is responsible for the more glass-like temperature dependence of the thermal conductivity, whereas more harmonic energy transfer at lower temperatures results in the experimentally observed crystal-like behaviour [31-33]. However, the differing cage structures in type II and H methane hydrate polymorphs led to less resonant scattering dissipating thermal transport, and more crystal-like behaviour [32]. The objective of the current study is to predict thermal conductivities in type II hydrogen hydrate using equilibrium molecular dynamics (MD) [35], and to investigate in detail the influence and importance of (guest-host) energy transfer processes thereon as well as those of the host lattice, with a particular focus on the temperature dependence of the thermal conductivity and the mechanisms governing this.

METHODOLOGY

In the MD simulation of hydrates, there exists some uncertainty as to the exact effect of a fixed-cage [5], in which the cage structure is immovable and the guest molecules are free, *versus* a flexible-cage [7], where the cage structure is free to distort. However, it is clear that there is a marked effect on energetic properties, for instance, from the differing guest-host interaction energies (-3.7 *versus* -2.2 kJ/mol

for singly-occupied large cages) obtained in refs. 5 and 7. Despite this, the fixed-cage approach is increasingly used in simulations due to its relative simplicity [36-38]. In this study, we adopt an approach similar to that of ref. 7, *i.e.*, using rigid H_2O molecules, and allowing them to move freely, *i.e.*, no restrictions on cage motion. Given that the best available potential models for H_2 hydrates are rigid-body, we use rigid-molecules for water and H_2. The water model used was TIP4P [39]. The parameterisation of Alavi *et al*. [40] was used for the charges and Lennard-Jones (LJ) interactions, along with geometric combining rules $\varepsilon^0_{ij} = (\varepsilon^0_{ii}\varepsilon^{0j}_{j})^{½}$, $\sigma^0_{ij} = (\sigma^0_{ii}\sigma^0_{jj})^{½}$, for water-guest and guest-guest LJ interactions. A sII hydrate 1088-H_2O molecule supercell, consisting of 2x2x2 unit cells, with the fundamental unit cell length ~17 Å [3] was constructed. The Bernal-Fowler rules [41] were used in selecting the initial orientation of the water molecules so that the total dipole moment would be vanishingly small, and the Rahman-Stillinger procedure was used to achieve a small total dipole moment [42]. Two systems were constructed, both with quadruple occupation in the large cavities, and single- and double-occupation in the small cages (dubbed '1s4l' and '2s4l', respectively). The guests' initial positions in the system were generated by mass-centring, *i.e.*, by placing the H_2 molecules around the cage centres at an energetically reasonable distance from each other and the cage.

The Ewald method was used to handle long-range electrostatic interactions [35,43]. The real-space cut-off distance for the Ewald method was 10 Å, and the screening parameter and the number of wavevectors were set such that the relative error in the Ewald summation was less than 1×10^{-5}. In practice, this led to the product of the screening parameter α and the real-space cut-off distance to be in the range of around 3.2 to 3.5, and the Ewald electrostatic energy and forces varied very little with α and increasing number of wavevectors. The van der Waals cutoff distance was 8 Å. Rigid

constraints for the H_2O and H_2 were employed which implement the NOSQUISH algorithm of Miller *et al*. [44], using velocity-Verlet [45] integration with a 1 fs time-step. For system relaxation, 0.2 ns of Nosé-Hoover [46] NVT simulations at 30, 50, 100, 150, 200 and 250 K were performed for each system, and a rather mild 0.5 ps thermostat relaxation time. These were followed by 0.5 ns NPT [46, 47] runs at 0.05 kbar, with thermostat and barostat periods of 0.5 and 2 ps respectively, to allow each system volume to stabilise. Independent NVE production runs were then performed at each stable system volume for each system for 2 ns, and the temperature and pressure remained within 2 % of those established in the previous equilibration runs.

It should be pointed out that the use of classical MD to treat hydrogen molecules' motion, in particular, below around 100-150 K is approximate in nature, and the lack of provision of quantum effects like zero-point H_2 cage-rattling motions and quantisation of H_2 rotational motion, becomes less satisfactory at lower temperature. Bačić et al have studied these effects in much detail for hydrogen-containing clathrates [48-54], including explicit path-integral MD simulation [54]; based on these studies, it should be stressed that the classical MD results at 100 K and below reported in the present work needs to be interpreted with some caution due to the limitations of classical MD to describe accurately H_2 motion at low temperatures. Therefore, the present work seeks to describe only a classical approximation to hydrogen behaviour in clathrate systems, and seeks qualitative insights into dynamical and energetic properties underpinning thermal conduction; consequently, the results at 30, 50 and 100 K are necessarily somewhat tentative.

The heat flux vector **J** was evaluated by the microscopic expression in the molecular representation [55,56]:

$$V\mathbf{J} = \sum_{i=1}^{N} \mathbf{v}_i^{\text{c.m.}} e_i + \frac{1}{2} \sum_{i=1}^{N} \sum_{a=1}^{n_i} \sum_{j=1}^{N} \sum_{b=1}^{n_j} \mathbf{r}_{ij}^{\text{c.m.}} \mathbf{f}_{ia,jb} \cdot \mathbf{v}_{jb} - \sum_{\nu=1}^{2} h_\nu \sum_{i}^{N_\nu} \mathbf{v}_{i_\nu} \quad (1)$$

where N is the total number of molecules, and υ denotes the species (water or methane). In the diffusive term, e_i refers to the internal energy of molecule i (i.e. the sum of its kinetic energy and its interaction energy with the rest of the system). In the interactive term, there is a pairwise summation over the forces exerted by atomic sites on one another. The species enthalpy correction term requires that the total enthalpy of the system is decomposed into contributions from each species (water and hydrogen) [56]. Due to the partial transformation from pairwise, real-space treatment to a reciprocal space form in Ewald electrostatics, it is necessary to recast the diffusive and interactive terms in this expression in a form amenable for use with the Ewald method. This was done using the reformulation of Petravic [57]. It has become known recently that truncations of long-range electrostatic interactions in charged systems lead to errors in the stress tensor [58], and this shortcoming may affect the heat flux vector and its ACF markedly [27, 57]. Therefore, the use of Ewald electrostatics with Petravic's reformulation was required for accurate treatment in this study, based on previous validation of electrostatics methods for methane hydrates [27, 31-33] and amorphous ices [59, 60]. The heat flux vector was sampled every 1 fs in the production simulations.

The thermal conductivity was evaluated by the Green-Kubo time-correlation integral [61], of the autocorrelation function of the heat flux vector (JACF)

$$k = \frac{V}{3k_B T^2} \int_0^\infty \langle \mathbf{J}(t) \cdot \mathbf{J}(0) \rangle dt \quad (2)$$

The JACF was defined for 100 ps at 30 K, for 50 ps at 100 and 150 K and for 20 ps at 200 K and above; a sampling ratio of approximately 20:1 or higher is recommended for a robust definition of the ACF [26]. These durations were found to be more than

sufficient to provide a reliable estimate of the thermal conductivity at each temperature: the JACF had decayed essentially to zero within less than a quarter of the sampled time scales, and oscillated about zero thereafter. Romberg integration was used to evaluate eqn. 2, with smooth cubic spline interpolation to generate the required artificial JACF values in between the sampling intervals [62].

Relaxation times, related to energy transfer times between neighbouring atoms for phonon transport, may be extracted by fitting JACFs to sums of exponentially decaying functions, together with cosine-modulated terms for optic component decay [63, 64]. The normalised JACFs were decomposed as follows

$$JACF(t) = \sum_{i=1}^{n\_ac} A_i \exp(-t/\tau_i) + \sum_{j=1}^{n\_opt} \left(\sum_{k=1}^{n\_o,j} B_{jk} \exp(-t/\tau_{jk}) \right) \cos \omega_{0,j} t + \sum_{j=1}^{n\_opt} C_j \cos \omega_{0,j} t \quad (3)$$

where there were either two or three phonon (as opposed to 'lattice') acoustic modes (short-time, longer-time and, possibly, medium-time), depending on hydrate occupation and temperature, and the optical modes were gauged with reference to peaks in the optical region of the power spectrum obtained from the Fourier transform (FT) of the JACF. The fitting procedure is described in detail in previous studies [31,32]. The constant-amplitude term was applied to the optic modes to express the residual oscillation of the JACF about zero beyond the decay of the acoustic and optic modes, although it would be perhaps better to rationalise this as residual lattice acoustic modes (circa 0.3-0.65 ps), modulated by optic mode oscillation. Here, $\omega_{0,j}$ are the optical peaks from the JACF's power spectrum (i.e. 500 to 1000 cm^{-1} range). In practice, it was found that there was one main optical frequency mode (the main optic peak of the JACF's power spectrum) subject to relaxation, although there may have been more than one constant-term optic mode taken.

RESULTS AND DISCUSSION

A. System Densities

The densities and simulation-box dimensions of both systems are specified in Table I. The densities have a range of 851-933 kg/m^3. It can be seen readily that double occupation of the small cavity (the 2s4l case) leads to a lower density (due to a larger system volume as the two hydrogen molecules cause the small cages especially to expand somewhat); this is seen clearly in the larger box dimensions for the 2s4l system in Table I. In all cases, however, the cage structure remained intact. Mao et al found experimentally that the lattice parameter was *circa* 17.05 Å for hydrogen hydrate at 234 K and about 220 MPa, and the results in Table II are in reasonable agreement with experimental data [4]. In addition, it is evident in Table II that the 2s4l densities are somewhat lower than those of 1s4l, due to the volume expansion induced by double-occupation of the small cages vis-à-vis single-occupation; this mirrors similar findings of Alavi et al from MD simulations [65], whose lattice parameters at 160 and 250 K are similar to those of this study.

[insert Table I about here]

B. Cage radii

In addition to probing the system densities and box dimensions, the cage radii were determined. The instantaneous radius $r_i(t)$ for cage i was defined as the averaged distance of each constituent water molecules' centre-of-mass from the hypothetical 'centre-point' of each cage, with the central point $r_C(t)$ computed from the sum of the constituent water molecules' centres of mass, *i.e.*,

$$\mathbf{r}_{C,i}(t) = \sum_{j=1}^{N_{T,i}} \mathbf{r}_j(t) \qquad (4)$$

where $N_{T,i}$ denotes the number of constituent water molecules in the cage *i* of type T (*i.e.*, 20 for the small cavity and 28 for large cages). As mentioned previously, the cages were found to be stable in structure throughout, and the identity of the constituent water molecules remained constant.

The time-averaged cage radii are reported in Table II. As expected, the radii increase with increasing temperature. The radii of the doubly-occupied small cages is around 1 - 2 % larger than their singly-occupied counterparts, with the disparity increasing at higher temperatures; the corresponding result is about 1.5 % for large cavities. The general lattice expansion at higher temperatures (as characterised by decreasing overall system densities, cf. Table I) leads to a marginally greater local expansion in doubly-occupied small cavities. The cage radii are in good agreement with respective experimental data for small and large sII cage radii of 3.90 and 4.68 Å [66] and 3.91 and 4.73 Å [67]. However, this experimental data is close to the 250 K temperature range, and is not specifically for hydrogen hydrates; therefore, quantitative comparison with hydrogen hydrate cage radii is necessarily limited.

[insert Table II about here]

C. Thermal Conductivities

The computed thermal conductivities are illustrated in Fig. 1. Prior to discussing the conductivity results, however, it is worthwhile making some general remarks about crystalline thermal conductivity behaviour, the temperature profile of which is well-known: above half the Debye temperature, $\Theta_D/2$, the thermal conductivity exhibits a T^{-1} dependence, explained by Umklapp processes scattering phonons [68,69]. (For methane hydrate, Θ_D is 226 K [70], although this is a sI hydrate.) Thermal

conductivity increases as temperature decreases below $\Theta_D/2$, reaching a maximum near $\Theta_D/10$. In this "intermediate" régime, the thermal conductivity's absolute value is dependent heavily on defects. Below around $\Theta_D/10$, conductivity has a T^3 dependence, determined mainly by boundary scatterings. Therefore, experimental determination of thermal conductivity is highly dependent on samples' nature and quality, as outlined in some detail for hydrates [26-34], which serves to emphasise the difficulty in direct, quantitative comparisons of theoretical and experimental values, as previous research for hydrates has shown [26-24]. It must also be borne in mind that experimental measurements of hydrogen hydrate thermal conductivity have not been reported. It should also be noted that classical theory is expected to be valid at temperatures above one-tenth of the Debye temperature ($\Theta_D/10$), but that this observation may be somewhat tentative for hydrogen hydrate, in view of the previously mentioned drawbacks of classical MD below 100-150 K, e.g., the lack of provision of quantum effects like zero-point H_2 cage-rattling motions and quantisation of H_2 rotational motion. Bearing these factors in mind, the essential aim of this study is to uncover the qualitative trend in the temperature dependence of 1s4l and 2s4l thermal conductivity, and elucidate the underlying microscopic mechanisms governing this behaviour.

[insert Figure 1 about here]

The temperature profile of 1s4l hydrate displays a largely crystalline one, in marked contrast to the doubly-occupied small cavity (2s4l) (cf. Fig. 1), which displays a lower conductivity, but, interestingly, a crystal-like temperature profile below around100-150 K and a more amorphous-like temperature dependence above this. These

observations are consistent with expectations, when one reflects on findings of similar MD studies for methane hydrates [31-33]: greater damping of guest-host energy transfer in type I methane hydrates above 150 K was found to lead to more glass-like temperature dependence of the thermal conductivity, whereas more harmonic energy transfer at lower temperatures results in experimentally observed crystal-like behaviour [31-33], whereas differing cage structures in type II methane hydrate polymorphs led to less resonant scattering dissipating thermal transport, and more crystal-like behaviour [32]. It would appear that the double occupation of the small cavities in the 2s4l system, and resultant closer contact between these H_2 molecules and the host, leads to greater damping in guest-host energy transfer at higher temperatures (above 100-150 K, say), leading to a more glass-like temperature dependence, while the reduced coupling of H_2 and the host lattice in singly-occupied small cages (1s4l) leads to more harmonic guest-host energy transfer. Also, the thermal conductivities are somewhat larger in magnitude for both hydrogen hydrates (particularly 1s4l) than even high-pressure type II methane hydrates [32], and this would appear to be attributable to less resonant scattering of phonons by the smaller H_2 molecules than methane. To investigate this further, guest and host power spectra and guest-host energy transfer correlation functions shall be analysed in sections E and F, respectively, following a further discussion of the nature of different contributions to the thermal conductivity and associated thermal conduction relaxation times in section D.

D. Analysis of Heat Flux ACFs

As mentioned previously, the heat flux correlation function can be partitioned into acoustic and optic components. The acoustic part was obtained via reverse

transformation of the low-pass filtered Fourier transform, omitting the optical region (identified above 350-400 cm^{-1} in the power spectrum) [31,32]. The optic modes contribution is obtained by simply removing the acoustic component from the total JACF. The relaxation times, parameters, optic modes' frequencies and terms' contributions to the overall predicted thermal conductivity obtained from fittings to the JACF are provided in Table III, and sample JACFs are provided in Fig. 2 at 200 K for 1s4l and 2s4l systems. It is apparent in Fig. 2 that there is an intermediate relaxation time present for the 2s4l system, in contrast to that of the 1s4l case.

[insert Figure 2 and Table III about here]

The short-range acoustic relaxation times ($\tau_{sh,ac}$) decrease at higher temperatures, as expected due to more rapid local energy exchange within the lattice and between guest and lattice at higher temperatures. $\tau_{sh,ac}$ are consistently larger for the 1s4l (single-occupation of small cage) than 2s4l (double-occupation), with the disparity growing as temperature increases (some 5 % larger at 30 K, but 70 % larger at 250 K). For the 2s4l case, $\tau_{sh,ac}$ are dramatically lower at temperatures higher than 100 K. The long-range acoustic relaxation time ($\tau_{lg,ac}$) exhibits a more gradual reduction for both systems as temperature increases, with similar results for each system; this term is dominated largely by the behaviour of the host lattice [31-33], which is similar for both systems (cf. host translational and librational spectra in section D). For 1s4l (singly-occupied small cavity), a two-term acoustic fit (short- and long-range acoustic, $\tau_{sh,ac}$ and $\tau_{lg,ac}$) is adequate [31-33,63,64], as is the case for the doubly-occupied case (2s4l) below 100 K. For the 2s4l system at and above 150 K, a unique additional intermediate-range relaxation time ($\tau_{int,ac}$) achieves a better fit, as observed

in the case of higher-temperature damping of sI methane hydrate [31-33]. $\tau_{int,ac}$'s magnitude (when present at and above 100 K for doubly-occupied small cages) is between $\tau_{sh,ac}$ and $\tau_{lg,ac}$ and is relatively insensitive to temperature (~0.3-0.4 ps), albeit subject to comparatively larger statistical uncertainty. It is worth remarking at this point that earlier analysis of tetrahydrofuran hydrate's conductivity with the resonant scattering model required an additional effective relaxation time of ~0.1 ps to describe heat dissipation via guest rattling [17]. Furthermore, the calculated lifetimes of strongly scattered phonon modes in Xe hydrate are 0.3-1.0 ps [21]. This suggests that the higher-temperature medium-range acoustic relaxation times in the doubly-occupied small cages of the 2s4l hydrate arise from guest-host coupling.

The acoustic and optic relaxation results in Table III also include contributions arising from analytic integration of the fitted parameters to the normalized JACF, in eqn. 3 (also see refs. [31-33]). These are obtained from the zero-frequency values of the analytic real FT. The largest contribution to the thermal conductivity is derived from the long-range, low-frequency acoustic term, which is dominated by the behaviour of the host lattice [31-33]. In 2s4l hydrate at and above 150 K, the short and intermediate terms contribute (cf. Fig. 2), with the former being about 1.4-2.25 times larger than the latter, but the latter growing in magnitude at higher temperatures. This is somewhat similar to sI methane hydrate [31-33] at higher temperatures (at and above 150 K), except in that case the short- and medium-range acoustic terms are approximately equal in importance and a shallow minimum in predicted thermal conductivity is observed in the vicinity of 150 K (along with lower conductivity than 2s4l hydrate), owing to a greater extent of damping of guest-host energy transfer due to the larger size of the (single) methane molecule than by the thermal-activated motion of two hydrogen molecules. For both 1s4l and 2s4l hydrates, the optic

contribution is in the 10-15% range, which is in agreement with *ca*. 10 % estimated from high-quality experimental data for ice Ih [71].

E. Velocity correlation functions

Normalised velocity auto-correlation functions (VACF's) measure the degree of significance of coupling of atomic motions with themselves. These were calculated for each atom type, *i*

$$Z_{ii}(t) = \langle \mathbf{v}_i(0) \cdot \mathbf{v}_i(t) \rangle / \langle \mathbf{v}_i(0) \cdot \mathbf{v}_i(0) \rangle \quad (5)$$

The frequency modes of the VACFs contributing to motion are revealed via their power spectra (FTs). Velocity cross-correlation functions (VCCFs) are defined as

$$Z_{ij}(t) = \langle \mathbf{v}_m(0) \cdot \mathbf{v}_n(t) \rangle \; / \; (\langle \mathbf{v}_m(0) \cdot \mathbf{v}_m(0) \rangle^{1/2} \langle \mathbf{v}_n(0) \cdot \mathbf{v}_n(0) \rangle^{1/2}) \quad (6)$$

where $m \neq n$. If the motions of guests are entirely localised and independent of lattice vibrations, the VCCF between guest and water will be damped rapidly and the VCCF's power spectrum shall be featureless. In contrast, if the motions of the water lattice and the guests are completely correlated, features in the FT of the VCCF will resemble the power spectrum of the individual components.

Selected host- and guest- power spectra (from VACFs) are shown in Figs. 3 and 4 for the 1s4l and 2s4l systems, respectively. H_2 in the small and large cages are treated separately, and referred to as SH_2 and LH_2 respectively. For the host translational density of states (DOS), *i.e.*, the OW spectrum, it is thought [17,20,21] that the peak at about 60 to 110 cm^{-1} corresponds to transverse acoustic phonons propagating along directions of high symmetry at the boundary of the Brillouin zone, while the higher frequency secondary peak at 300-400 cm^{-1} is thought to be attributable to longitudinal and transverse optical modes. The power spectra of the hydrogens in the water molecules of the host lattice, *i.e.*, the librational DOS, are depicted in the insets of

Figs. 3 and 4 at 30 and 200 K; the librational density of states span the frequency range of 400 to 1250 cm^{-1}, and are separated from the translational DOS by a well-defined frequency gap. The temperature dependence of the spectra exhibits a circa 30-50 cm^{-1} shift between 30 and 200 K. In general (cf. Figs. 3 and 4), the H_2 spectra depict a certain extent of overlap between both the host's lattice transverse acoustic and optical modes, but, at 200 K, move closer towards greater overlap with the lattice transverse acoustic mode, owing to greater collisions at higher temperature with the neighbouring cage-water molecules; this was confirmed by a greater overlap in the H_2-OW VCCF spectrum at 200 K. More specifically, in Fig. 3 at 30 K, both the SH_2 and LH_2 (on a COM basis, *i.e.*, the single H_2 in the small cavity and quadruple H_2 in the large cage) possess vibrational modes at about 305 and 410 cm^{-1}, respectively. At 200 K, the SH_2 vibrational modes shift downwards to about 150-170 cm^{-1}, closer to the lattice transverse acoustic mode. It can be seen that the H_2 spectra in the large cages are quite similar at 200 K for both 1s4l and 2s4l systems, with a frequency mode of *circa* 190 cm^{-1}, and the 1s4l and 2s4l LH_2 spectra are again essentially in agreement at 30 K (cf. Figs. 3b and 4b); similar dynamics in the large cages with quadruple occupation in both systems would be expected. In Fig. 4, for the 2s4l system, a high degree of coupling is evident at 30 K between double-occupation SH_2 and quadruple-occupation LH_2 with the lattice longitudinal and transverse optical modes at about 400-415 cm^{-1}. However, at 200 K, the increase in overlap of H_2 modes in the 160-230 cm^{-1} range with the lattice optical modes is more evident vis-à-vis 30 K, especially for the double-occupation SH_2 case. The tendency for H_2 vibrational coupling with lattice optical modes appears to be a signature of multiple H_2 occupation, for both large and small cages, with a particular thermally activated increase in overlap in the doubly-occupied small cages, due to more intimate

coupling in motion with closer contact between both of the hydrogen molecules and the surrounding host water molecules. Further evidence for this coupling lies in the SH_2 case in Fig. 4b at 200 K in the 2s4l system, with the peak at circa 650 cm^{-1} arising due to coupling of the H_2 molecules in the small cavity with librational modes of the water molecules (seen in the inset in Fig. 4b for the waters' protons). This occurs due to the higher-temperature activation of this higher-frequency coupling with the more intimate hydrogen-water contact of doubly-occupied small cavities.

[insert Figures 3 & 4 about here]

The shift to lower energies at 200 K of the lattice transverse acoustic mode (labelled 'OW' for waters' oxygen atoms) is evident upon increasing the hydrogen small cage occupation from single (Fig. 3b) to double (Fig. 4b). This is indicative of a shift towards a weaker, or more strained, hydrogen bond arrangement in the 2s4l system vis-à-vis the 1s4l case. This results in greater inhibition of long-range modes and spatial localisation in energy [31,32], which may be expected to contribute to a more amorphous-like temperature dependence of the thermal conductivity in 2s4l; indeed, this phenomenon has been observed in methane hydrates.

It is both useful and relevant to compare and contrast inelastic neutron scattering (INS) results for quantum rattling motions of the hydrogen molecules in binary THF/H_2 hydrates of Ulivi *et al.* at 20 K [72] with the SH_2 and LH_2 power spectra in Figs. 2 and 3. Unfortunately, due to the classical nature of the MD used in this study, it is not possible to capture the INS-observed rattling fundamental or rotation modes due to various quantum motions, *e.g.*, the strong $J = 0 – 1$ and $J = 1 - 1$ transitions at 71-101 cm^{-1} and 110-122 cm^{-1} [72]. As remarked previously, the goal of this study is

to achieve a qualitative understanding for energy transfer and thermal conduction in hydrogen hydrates, but full path-integral MD simulation would be of benefit in the future in allowing quantum effects on nuclear motion to be incorporated, as Witt *et al.* [54] have done recently, although this would still be challenging for treatment of quantum rattling modes.

F. Energy correlation functions

Interaction energies of the H_2 guests with the water lattice and the rest of the system were calculated, using Lekner electrostatics [73,74] for the Coulombic component, where the H_2 in the small and large cages are treated separately, and referred to as SH_2 and LH_2 respectively, as previously. To investigate the underlying magnitude and dynamics of energy transfer processes, in particular guest-host transfer, the autocorrelation function of the guest-host interaction energy was defined, averaged out for SH_2 and LH_2. For a purely harmonic system, there is no energy dissipation due to energy transfer between two subsystems. The energy is simply exchanged back and forth between the subsystems and the interaction energy ACF would resemble a harmonic oscillator with essentially no change in the amplitude with time. On the other hand, if energy is dissipated, the amplitude of the ACF will be attenuated (damped) by a decreasing exponential function characterised by the relaxation time of the process. The normalised guest-host energy ACF was defined as

$$ECF_{gh}(t) = < U_{gh}(t) U_{gh}(0) > / < U_{gh}(0) U_{gh}(0) > \qquad (7)$$

and these are depicted in Figs. 4 and 5 for 1s4l and 2s4l systems.

[insert Figs. 4 and 5 about here]

It was found that there was essentially periodic variation in the guest-host interaction energy in the case of the small, singly occupied cage in the 1s4l system at all temperatures (cf. Fig. 5), with a period of circa 6 ps, indicating largely harmonic transfer in that case; in sI methane hydrate, similar transfer times were observed [32]. However, for quadruple occupation in the large cavities, there was little evidence of harmonicity in energy transfer, *i.e.*, guest-host energy transport is damped. In the case of the 2s4l system with double occupation of the small cage, Fig. 6 shows that energy transfer displays little periodicity. The more intimate guest-host contact mediated via closer contact for double occupation in small cages leads to a greater extent of damping, and this is confirmed further by the power spectra results, particularly at higher temperature (cf. Fig. 4, especially in Fig. 4b showing SH_2 librational coupling with the waters' proton rotational oscillation at around 650 cm^{-1}). This occurs due to the higher-temperature activation of this higher-frequency coupling with the more intimate hydrogen-water contact of doubly-occupied small cavities. This is also supported by the appearance of an intermediate relaxation time for thermal conduction at and above 150 K for the 2s4l system. As reported previously for methane hydrate [31-33], it is the guest-host interactions that tend to determine the temperature dependence of the thermal conductivity, while it has been conjectured that the more strained hydrogen bonding in the hydrate lattice vis-à-vis ice Ih leads to lower thermal conductivity itself. These earlier findings are relevant for this study, in that the double contact of the small cage and thermally activated closer overlap in motion and damping of energy transfer leads to higher-temperature amorphous-like thermal conductivity behaviour, unlike the crystalline behaviour of singly-occupied small cages in 1s4l hydrate.

G. Inter-cage hydrogen migration

Senadheera and Conradi have recently studied the nature of H_2 guest motions in TDF/H_2 D_2O clathrates by analysing the temperature dependence of their NMR line-shapes [75,76]. Although it would be of interest to compare directly the resultant NMR-derived relaxation times with the MD simulations of this study, the experimentally relevant timescales are simply too extended for molecular simulation to probe adequately. However, Senadheera and Conradi [76] commented that the NMR results appeared to suggest larger energy barriers towards inter-cage hydrogen diffusion vis-à-vis experimental observations of H_2 diffusion in TDF/H_2 D_2O clathrates of Okuchi *et al.* [77], and more in line with experimental data of Mulder *et al.* [78]. Bearing in mind these direct experimental observations of H_2 diffusion in clathrates [77,78], together with electronic structure observations of Alavi and Ripmeester [79,80] to characterise energy barriers and diffusion pathways, and direct observation of inter-cage H_2 diffusion in classical MD simulations of Frankcombe and Kroes [81], there is an open question as to the possible effect of H_2 inter-cage migration on thermal conduction. Therefore, we resolved to assess the extent of any inter-cage hydrogen migration in these MD simulations to ascertain if there is any possible influence on thermal conduction.

Hydrogen migration events were monitored by consideration of the evolution of the distance of each hydrogen molecule from the instantaneous centre of each cage of which it was part at the beginning of the simulation. Once this distance exceeded about 25 % greater than the cage radius of eqn. 4, this was classified as an inter-cage migration event, beyond intra-cage rattling or at pentagonal faces of the small cages of origin. Such ‘cage-hopping’ events were observed in this study only from and to doubly-occupied small cavities, leaving some small cavities only very temporarily

singly or triply occupied. Naturally, this is very temperature-dependent, and was only observed to occur to any extent in the 2s4l system at 250 K. It should be noted that the inter-cage migration events in 2s4l at 250 K coincide with the larger amplitude of fluctuations in the density of this system of ~ 3.5 kg/m^3 as compared to 0.8-1.1 kg/m^3 for other systems with essentially no observed inter-cage hydrogen migration (cf. Table II), along with a larger small-cage radius of 4.07 Å, which itself had larger fluctuations than the other observed cavity radii. Therefore, although inter-cage hydrogen diffusion would be expected to lead to very intimate water-H_2 contact and much more strained hydrogen bonding, giving in turn more amorphous-like behaviour in the thermal conductivity, it is only really a factor for the 2s4l system at 250 K. Reference to Fig. 1 does indeed show that there is essentially no decrease in thermal conductivity between 200 and 250 K for the 2s4l system, so the onset of inter-cage hydrogen migration may serve to explain, at least in part, this amorphous behaviour.

CONCLUSIONS

In this study, equilibrium MD simulations have been carried out to investigate the behaviour of thermal conductivity and its underlying microscopic origins in energy transfer processes, from 30 to 250 K at 0.05 kbar. As mentioned previously, at around 150 K and below, it is likely that classical MD will not capture the quantum nature of H_2 motion especially; however, this study does not have as its central aim the determination of absolute thermal conductivity with near-quantitative accuracy, but rather a more general qualitative understanding of thermal conduction behaviour and mechanisms, especially depending on cage occupancy and temperature. It was shown via damping in the guest-host interaction energy ACF, and the associated resonant

scattering of phonons, for double occupation in small cages leads, arising from more intimate guest-host contact (as confirmed further by power spectra) leads to more amorphous-like behaviour of the thermal conductivity at higher temperatures. This echoes findings from methane hydrates [31-33], where it was found that higher-temperature resonant scattering from guest-host interactions and damping of energy transfer led to amorphous-like behaviour of the thermal conductivity. In contrast, single occupation by H_2 of the small cage appears to lead to substantially less resonant scattering and more harmonic energy transfer, explaining the more crystalline behaviour of the thermal conductivity, and its larger value vis-à-vis 2s4l hydrate, and, in turn, sI methane hydrate.

ACKNOWLEDGEMENTS

This material is based upon works supported by the Science Foundation Ireland (SFI) under Grant No. [07/SRC/B1160], for the Solar Energy Cluster. The authors acknowledge useful discussions with Kevin O'Neill, John Tse and Peter Kusalik, and thank the travel support provided by the Ireland Canada University Foundation and Royal Irish Academy.

REFERENCES

[1] Y.F. Makogon, *Hydrates of Hydrocarbons,* PennWell Books, Tulsa, Oklahoma (1997).

[2] E.D. Sloan and C.A. Koh, *Clathrate Hydrates of Natural Gases*, 3rd rev. ed., CRC Press, Taylor & Francis USA (2007).

[3] G.A. Jeffrey and R.K. McMullan, *Prog. Inorg. Chem.*, **8**, 43–108 (1967).

[4] W.L. Mao, H. Mao, A.F. Goncharov, V.V. Struzhkin, Q. Guo, J. Hu, J. Shu, R.J. Hemley, M. Somayazulu and Y. Zhao, *Science*, **297**, 2247-2249 (2002).

[5] S. Patchkovskii and J.S. Tse, *PNAS*, **100**, 14645-14650 (2003).

[6] M.H.F Sluiter, H. Adachi, R.V. Belosludov, V.R. Belosludov and Y. Kawazoe, *Mater. Trans.*, **45**, 1452-1454 (2004).

[7] S. Alavi, J.A. Ripmeester and D.D. Klug, *J. Chem. Phys*, **123**, 024507 (2005).

[8] H. Lee, J. Lee, D.Y. Kim, J. Park, Y.T. Seo, H. Zeg, I.L. Moudrakovski, C.I. Ratcliffe and J.A. Ripmeester, *Nature*, **434**, 743-746, (2005).

[9] T.M. Inerbaev, V.R. Belosludov, R.V. Belosludov, M. Sluiter, Y. Kawazoe, J. Kudoh, *J. Incl. Phenom. Macrocycl. Chem.*, **48**, 55-60 (2004).

[10] H. Erfan-Niya, H. Modarress and E. Zaminpayma, *J. Incl. Phenom. Macrocycl. Chem.*, **70**, 227-239 (2011).

[11] L.J. Florusse, C.J. Peters and J. Schoonman, et al., *Science*, **306**, 469-471 (2004).

[12] E. Newson, TH. Haueter, P. Hottinger, F. Von Roth, G.W.H. Schere and TH.H.Schucan. *Inter. J. Hydrogen Energy*, **23**, 905-909 (1998).

[13] N.F. Grünenfelder, T.H. Schunan, *Inter. J. Hydrogen Energy* **14**, 579-586 (1989).

[14] L.J. Rovetto, T.A. Strobel, K.C. Hester, S.F. Dec, C.A. Koh, K.T. Miller and E.D. Sloan, *FY Annual Progress Report*, 2006.

[15] T. Nakayama, S. Tomura, M. Ozaki, R. Ohmura and Y.H. Mori, *Energy Fuels*, **24**, 2576–2588 (2010).

[16] R.G. Ross, P. Andersson and G. Bäckström, *Nature*, **290**, 322 (1981).

[17] J.S. Tse and M.A. White, *J. Phys. Chem.*, **92**, 5006 (1988).

[18] G.A. Slack. In *Thermoelectric Materials—New Directions and Approaches, Symp. Proc. Mater. Res. Soc.*, ed. TM Tritt, MG Kanatzidis, HB Lyon, GD Mahan, 478, 47–54. Pittsburgh: Mater. Res. Soc. (1997).

[19] G.S. Nolas, D.T. Morelli and T.M. Tritt, *Ann. Rev. Materials Sci.*, 89 (1999)

[20] J.S. Tse, C.I. Ratcliffe, B.M. Powell, V.P. Sears and Y.P. Handa, *J. Phys. Chem. A*, **101**, 4491 (1997).

[21] J.S. Tse, V.P. Shpakov, V.R. Belosludov, F. Trouw and Y.P. Handa, *Europhys. Lett.*, **54**, 354 (2001).

[22] J. Baumert, C. Gutt, V.P. Shpakov, J.S. Tse, M. Krisch, M. Müller, H. Requardt, D.D. Klug, S. Janssen and W. Press, *Phys. Rev. B*, **68**, 174301 (2003).

[23] J.S. Tse, D.D. Klug, J.Y. Zhao, W. Sturhahn, E.E. Alp, J. Baumert, C. Gutt, M.R. Johnson and W. Press, *Nature Materials*, **4**, 917 (2005).

[24] A.I. Krivchikov, B. Ya. Gorodilov, O.A. Korolyuk, V.G. Manzhelii, H. Conrad and W. Press, *J. Low Temp. Phys.*, **139**, 693-702 (2005).

[25] J.L. Cohn, G.S. Nolas, V. Fessatidis, T.H. Metcalf and G.A. Slack, *Phys. Rev. Lett.*, **82**, 779 (1999).

[26] E.J. Rosenbaum, N.J. English, J.K. Johnson, D.W. Shaw and R.P. Warzinski, *J. Phys. Chem. B*, **111**, 13194-13205 (2007).

[27] N.J. English, *Molec. Phys.*, **106**, 1887-1898 (2008).

[28] H. Jiang, E. Myshakin, K.D. Jordan and R.P. Warzinski, *J. Phys. Chem. B*, **112**, 10207 (2008).

[29] H. Jiang and K.D. Jordan, *J. Phys. Chem. C*, **114**, 5555-5564 (2010).

[30] N.J. English and J.S. Tse, *Energies*, **3**, 1914-1921 (2010).

[31] N.J. English and J.S. Tse, *Phys. Rev. Lett.*, **103**, 015901 (2009).

[32] N.J. English, J.S. Tse and D. Carey, *Phys. Rev. B*, **80**, 134306 (2009).

[33] N.J. English and J.S. Tse, *Comput. Mat. Sci.*, **49**, S176-S180 (2010).

[34] R. Inoue, H. Tanaka and K. Nakanishi, *J. Chem. Phys.*, **104**, 9569-9577 (1996).

[35] M.P. Allen and D.J. Tildesley, *Computer Simulation of Liquids*, Oxford (1987).

[36] M.Z. Xu, F. Sebastianelli and Z. Bačić, *J. Chem. Phys.*, **128**, 13-14 (2008).

[37] T.J. Frankcombe and G.J. Kroes, *J.Phys.Chem. C*, **111**, 13044-13052 (2007).

[38] S. Alavi and J.A. Ripmeester, *Angew. Chem., Int. Ed.*, **46**, 6102-6105 (2007).

[39] W.L. Jorgensen, D.S. Maxwell and J. Tirado-Rives, J. Amer. Chem. Soc., **118**, 11225 (1996).

[40] S. Alavi, J.A. Ripmeester and D.D. Klug, *J. Chem. Phys.*, **124**, 014704 (2006).

[41] J.D. Bernal and R.H. Fowler, *J. Chem. Phys.*, 1933, **1**, 515.

[42] A. Rahman and F.H. Stillinger, *J. Chem. Phys.*, 1972, **57**, 4009-4017.

[43] S.W. de Leeuw, J.W. Perram and E.R. Smith, *Proc. Royal Soc. London A,* **373**, 27 (1980).

[44] T. F. Miller, M. Eleftheriou, P. Pattnaik, A. Ndirango, D. Newns, and G. J. Martyna, *J. Chem. Phys.*, 2002, **116**, 8649-8659.

[45] W.G. Hoover, *Phys. Rev. A*, 1985, **31**, 1695-1697.

[46] H.C. Andersen, *J. Chem. Phys.*, 1980, **71**, 2384-2393.

[47] W.G. Hoover, *Phys. Rev. A*, 1986, **34**, 2499-2500.

[48] M. Xu, Y.S. Elmatad, F. Sebastianelli, J.W. Moskowitz and Z. Bačić, *J. Phys. Chem. B*, **110**, 24806 (2006).

[49] F. Sebastianelli, M. Xu, Y.S. Elmatad, J.W. Moskowitz and Z. Bačić, *J. Phys. Chem. C*, **111**, 2497 (2007).

[50] F. Sebastianelli, M. Xu, D.K. Kanan and Z. Bačić, *J. Phys. Chem. A*, **111**, 6115 (2007).

[51] M. Xu, F. Sebastianelli and Z. Bačić, *J. Phys. Chem. A*, **111**, 12763 (2007).

[52] M. Xu, F. Sebastianelli and Z. Bačić, *J. Chem. Phys.*, **128**, 244715 (2008).

[53] M. Xu, F. Sebastianelli and Z. Bačić, *J. Chem. Phys.*, **129**, 244706 (2008).

[54] A. Witt, F. Sebastianelli, M.E. Tuckerman and Z. Bačić, *J. Phys. Chem. C*, **114**, 20775 (2010).

[55] P.J. Daivis and D.J. Evans, *Molec. Phys.*, **81**, 1289 (1994).

[56] R. Vogelsang and C. Hoheisal, *Phys. Rev. A*, **35**, 3487 (1987).

[57] J. Petravic, *J. Chem. Phys.*, **123**, 174503 (2005).

[58] N. Galamba, C.A. Nieto de Castro and J.F. Ely, *J. Phys. Chem. B*, **108,** 3658 (2004).

[59] N.J. English and J.S. Tse, *Phys. Rev. B*, **83**, 184114 (2011).

[60] N.J. English, J.S. Tse and R. Gallagher, *Phys. Rev. B*, **82**, 092201 (2010).

[61] D.J. Evans and G.P. Morriss, *Statistical Mechanics of Nonequilibrium Liquids*, Academic Press, San Diego (1990).

[62] W.H. Press, B.P. Flannery, S.A. Teukolsky and W.T. Vetterling, *Numerical Recipes.* 2nd Ed., Cambridge Univ. Press, Cambridge, (1992).

[63] A.J.H. McGaughey and M. Kaviany, *Int. J. Heat Mass Transfer*, **47**, 1783 (2004).

[64] A.J.H. McGaughey and M. Kaviany, *Int. J. Heat Mass Transfer*, **47**, 1799 (2004).

[65] S. Alavi, D.D. Klug and J.A. Ripmeester, *J. Chem. Phys.*, **128**, 064506 (2008).

[66] E.D. Sloan, Jr., *Clathrate Hydrates of Natural Gases* (Marcel Dekker, New York, 1990).

[67] E.D. Sloan, Jr., *Nature*, **426**, 353 (2003).

[68] T.M. Tritt, *Thermal Conductivity: Theory, Properties, and Applications* (Kluwer Academic, Plenum Publishers, 2004).

[69] A.J.H. McGaughey and M. Kaviany, *Adv. Heat Transfer* **39**, 169 (2006).

[70] J.S. Tse, *J. Phys. Colloques* **48**, C1:543 (1987).

[71] G.A. Slack, *Phys. Rev. B* **22**, 3065 (1980).

[72] L. Ulivi, M. Celli, A. Giannasi, A.J. Ramirez-Cuesta, D. J. Bull and M. Zoppi, Phys. Rev. B **76**, 161401(R) (2007).

[73] J. Lekner, *Physica A*, **157**, 826 (1989).

[74] J. Lekner, *Physica A*, **176**, 485 (1991).

[75] L. Senadheera and M.S. Conradi, *J. Phys. Chem. B*, **111**, 12097 (2007).

[76] L. Senadheera and M.S. Conradi, *J. Phys. Chem. B*, **112**, 13695 (2008).

[77] T.Okuchi, I.L. Moudrakovski and J.A. Ripmeester, *Appl. Phys. Lett.*, **91**, 171903 (2007).

[78] F.M. Mulder, M. Wagemaker, L. van Eijck and G.J. Kearley, *ChemPhysChem*, **9**, 1331 (2008).

[79] S. Alavi and J.A. Ripmeester, *Angew. Chem. Int. Ed.*, **46**, 6102 (2007).

[80] S. Alavi and J.A. Ripmeester, *Chem. Phys. Lett.*, **479**, 234 (2009).

[81] T.J. Frankcombe and G.-J. Kroes, *J. Phys. Chem. C*, **111**, 13044 (2007).

T (K)	1s4l	2s4l
30	933.6 (33.09)	918.3 (33.41)
50	933.4 (33.09)	915.2 (33.45)
100	920.7 (33.24)	908.0 (33.54)
150	910.6 (33.37)	893.4 (33.72)
200	898.8 (33.51)	872.2 (33.99)
250	885.1 (33.68)	851.8[a] (34.26)

Table I. Comparison of the 1s4l and 2s4l (single- and double-occupation of the small cavity, respectively) densities (kg/m^3) at 0.05 kbar; the standard deviations are approximately 0.8-1.1 kg/m^3. The box dimensions of the 2×2×2 sII systems (double the lattice constant) are specified in Å in parentheses after the density. [a]Denotes that this state remains hydrate-like for the duration of the simulation, with all cages remaining intact, but the fluctuations in volume are somewhat larger, with a standard deviation of ~ 3.5 kg/m^3.

T (K)	Small 1s4l	Small 2s4l	Large 1s4l	Large 2s4l
30	3.89	3.93	4.67	4.74
50	3.89	3.93	4.68	4.74
100	3.90	3.96	4.70	4.77
150	3.92	3.99	4.74	4.81
200	3.94	4.02	4.80	4.87
250	3.99	4.07	4.88	4.96

Table II. Large and small cage radii (Å).

Type	T (K)	$\tau_{sh,ac}$ (ps)	Short-range acoustic	$\tau_{int,ac}$ (ps)	Medium-range acoustic	$\tau_{lg,ac}$ (ps)	Long-range acoustic	Optic	Total
1s4l	30	0.42± 0.059	0.33			4.9± .52	1.02	0.17	1.52± 0.062
	50	0.28± 0.037	0.28			4.0± .39	0.87	0.16	1.31± 0.060
	100	0.21± 0.019	0.24			3.6± .34	0.69	0.13	1.06± 0.063
	150	0.10± 0.019	0.19			3.1± .28	0.57	0.12	0.88± 0.057
	200	0.068± 0.008	0.17			2.3± .30	0.53	0.11	0.81± 0.053
	250	0.036± 0.005	0.14			2.0± .26	0.51	0.11	0.76± 0.052
2s4l	30	0.40± 0.053	0.30			4.7± .56	0.99	0.16	1.45± 0.064
	50	0.24± 0.039	0.26			3.9± .45	0.81	0.17	1.24± 0.063
	100	0.15± 0.021	0.14			3.4± .42	0.62	0.11	0.87± 0.058
	150	0.066± 0.012	0.09	0.34± 0.14	0.04	2.7± .36	0.51	0.10	0.74± 0.052
	200	0.039± 0.0067	0.08	0.30± 0.11	0.05	2.1± .29	0.50	0.09	0.72± 0.055
	250	0.021± 0.0038	0.07	0.33± 0.12	0.05	1.8± .22	0.50	0.09	0.71± 0.049

Table III. Acoustic relaxation times and contributions to the overall estimated thermal conductivity based on fitting procedure in $Wm^{-1}K^{-1}$.

FIGURE CAPTIONS

Figure 1. Computed thermal conductivities for the 1s4l and 2s4l systems (singly- and doubly-occupied small cavities, respectively) at 0.05 kbar

Figure 2. Heat flux vector autocorrelation function for the 1s4l and 2s4l systems (singly- and doubly-occupied small cavities, respectively) at 0.05 kbar and 200 K

Figure 3. Power spectra for the 1s4l system at (a) 30, (b) 200 K. The guest spectra are on a COM-basis. 'OW' and 'HW' refer to the spectra of the waters' oxygen and hydrogen atoms, respectively.

Figure 4. Power spectra for the 2s4l system at (a) 30, (b) 200 K. The guest spectra are on a COM-basis. 'OW' and 'HW' refer to the spectra of the waters' oxygen and hydrogen atoms, respectively.

Figure 5. Autocorrelation function of the hydrogen-host interaction energy in the 1s4l system at 30 and 200K.

Figure 6. Autocorrelation function of the hydrogen-host interaction energy in the 2s4l system at 30 and 200K.

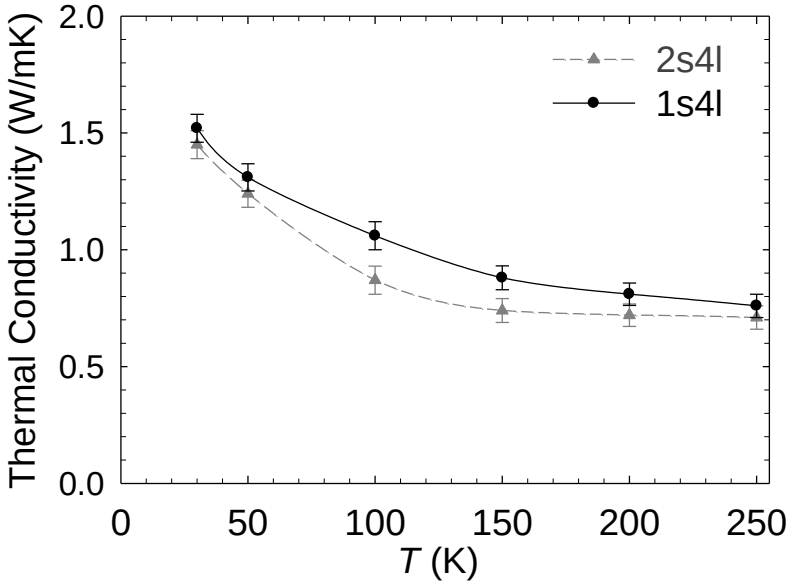
Thermal Conductivity (W/mK)
2.0
1.5
1.0
0.5
0.0
0
50
100
150
200
250
T (K)
2s4l
1s4l

Fig. 1

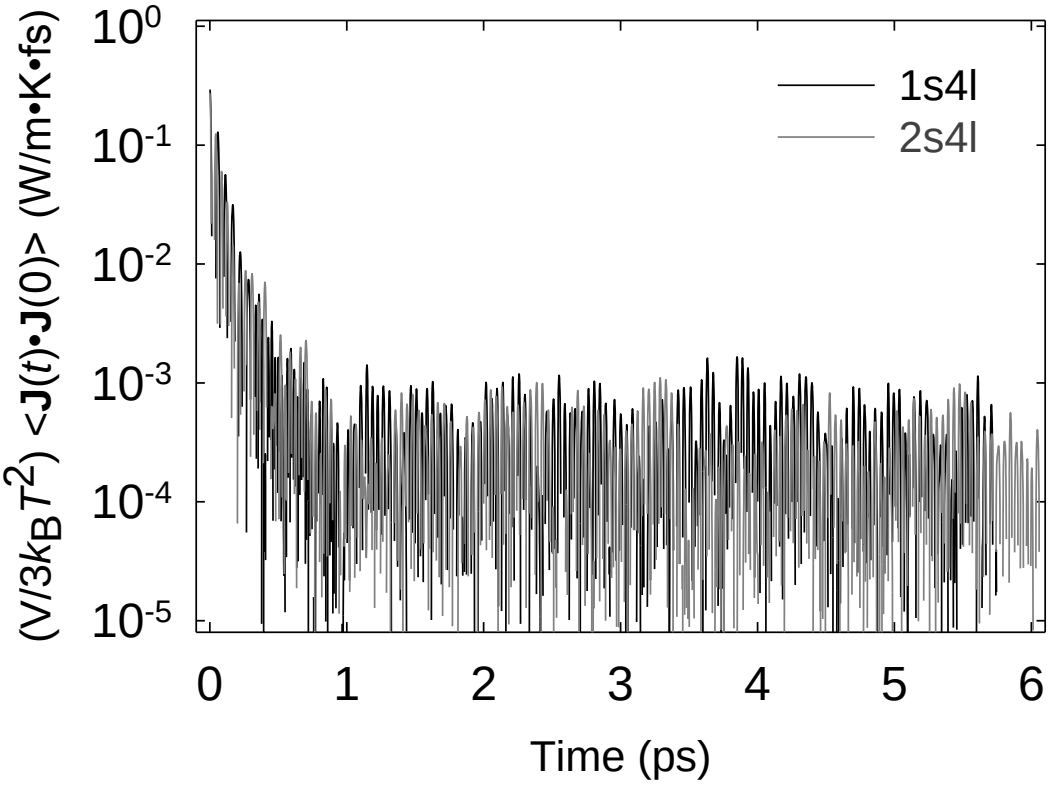
$(V/3k_BT^2)$ <**J**(*t*)•**J**(0)> (W/m•K•fs)
10^0
10^{-1}
10^{-2}
10^{-3}
10^{-4}
10^{-5}
0
1
2
3
4
5
6
Time (ps)
1s4l
2s4l

Fig. 2

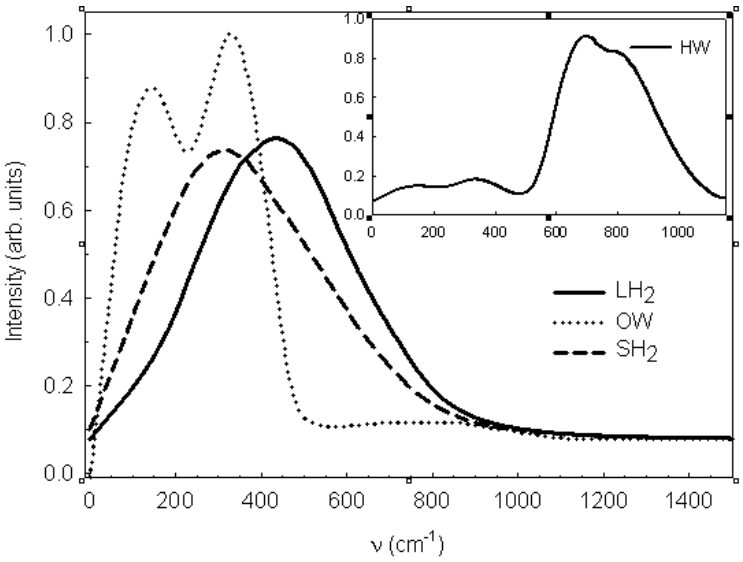

Fig. 3a FT-VACF 1s4l 30K

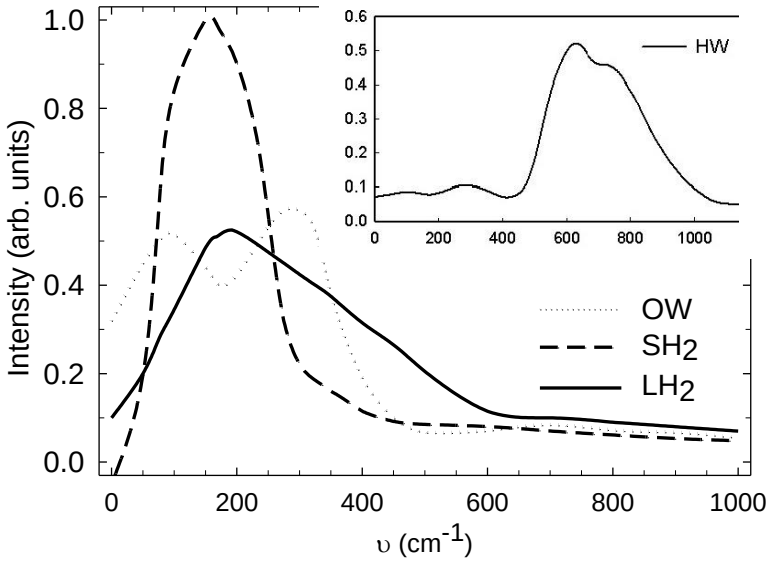

Fig. 3b FT-VACF 1s4l 200K

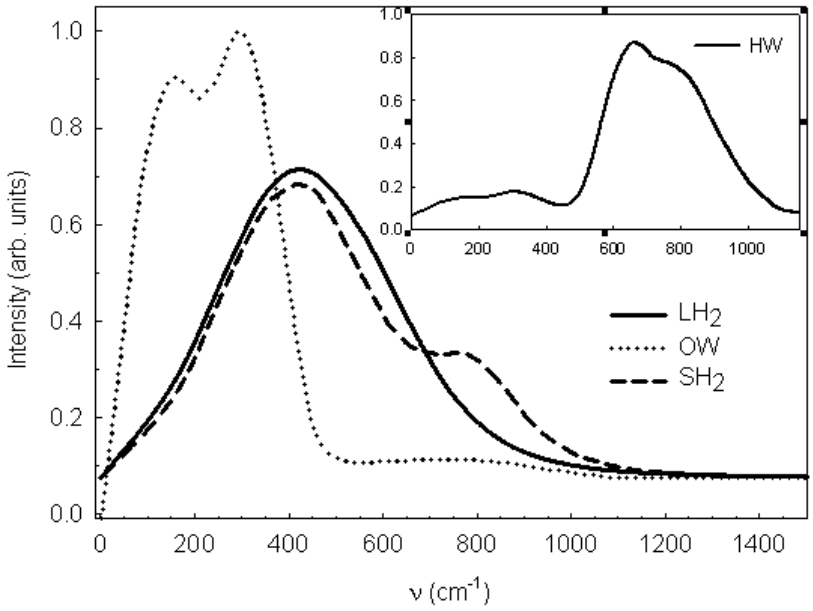

Fig. 4a FT-VACF 2s4l 30K

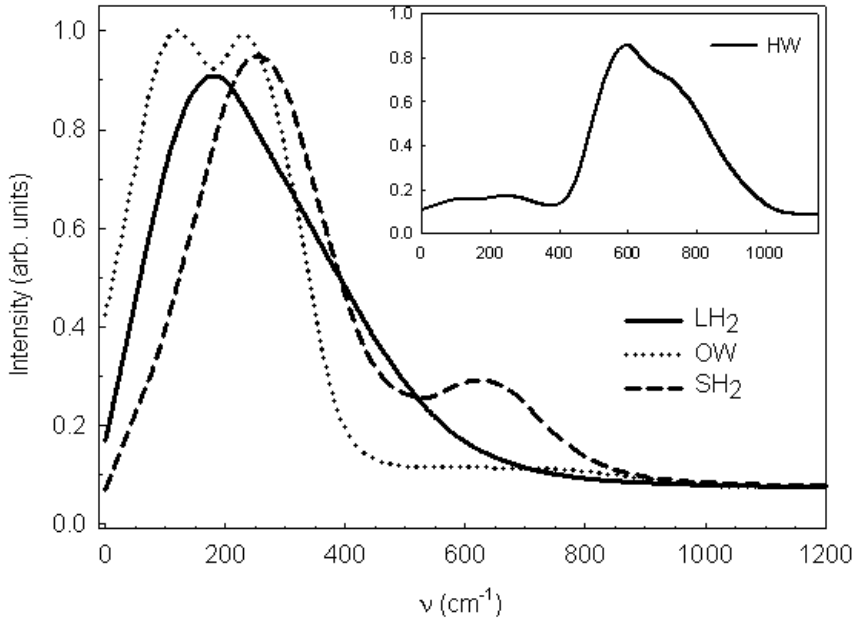

Fig. 4b FT-VACF 2s4l 200K

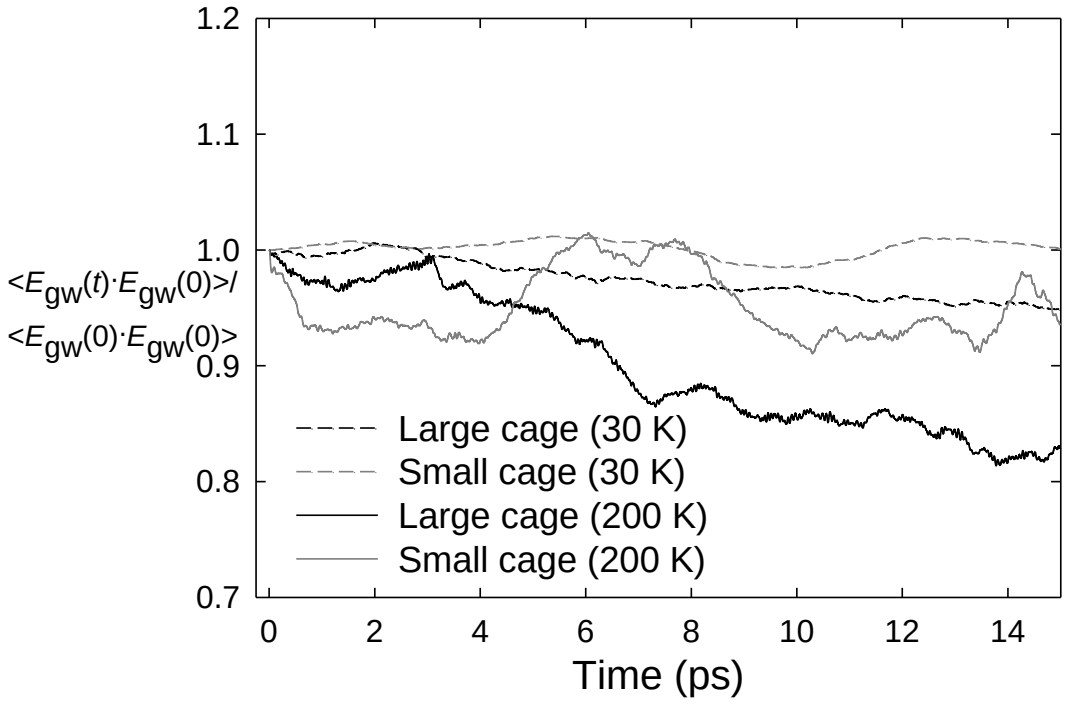

Fig. 5 Guest-host energy ACF 1s4l

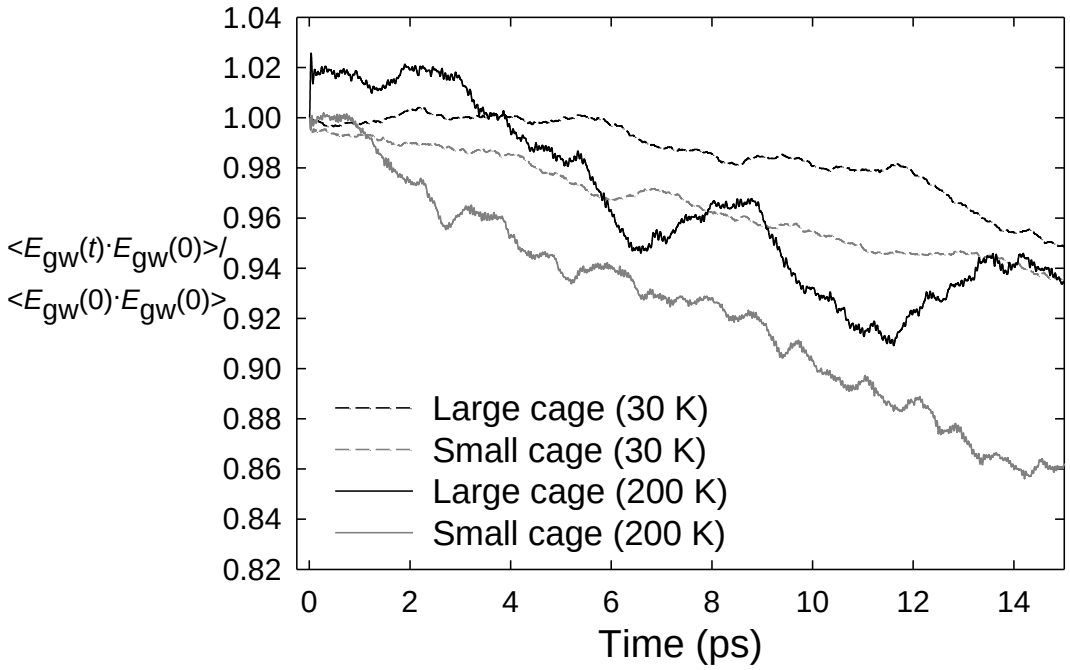

Fig. 6 Guest-host energy ACF 2s4l